Design of a High-Concentration Microtracking Photovoltaic System

Gregory S. Brulo
Department of Mechanical Engineering,
The Pennsylvania State University,
University Park, PA 16802
e-mail: gbrulo@gmail.com

Alex J. Grede
School of Electrical Engineering and Computer Science,
The Pennsylvania State University,
University Park, PA 16802
e-mail: ajg324@psu.edu

Andrew J. Ren
School of Electrical Engineering and Computer Science,
The Pennsylvania State University,
University Park, PA 16802
e-mail: ajr5777@psu.edu

Christopher D. Rahn
Department of Mechanical Engineering,
The Pennsylvania State University,
University Park, PA 16802
e-mail: cdrahn@psu.edu

Noel C. Giebink
School of Electrical Engineering and Computer Science,
The Pennsylvania State University,
University Park, PA 16802
e-mail: ncg2@psu.edu

High-concentration photovoltaic systems can provide power conversion efficiency that is nearly double that of conventional solar panels. Concentrating photovoltaics (CPV) cannot compete with fixed silicon panels for rooftop installations due to the complexity and cost of CPV two-axis pedestal tracking systems. Fixed optic designs have recently been proposed to have a transparent middle sheet with small, widely spaced, and highly efficient solar cells sandwiched between a fixed lenslet array on the top and a fixed reflector array on the bottom. Precision actuators position the middle sheet at the focal points of the lenslet/reflector array to microtrack the sun throughout the day. This paper discusses the kinematic design and control of shape memory alloy (SMA) actuators used for the first time in this solar microtracking application. SMA actuators have the potential to be less expensive, easier to integrate, and lower power than electric motors. The kinematic design maintains upper and lower bounds on wire tension to prevent failure and ensure reversible actuation, respectively. The SMA actuators under quasi-linearized proportional integral directive (PID) control can position the middle sheet with ± 7 mm of range in the vertical and horizontal directions while ensuring less than 1.9 μm of steady-state error in SMA actuator stroke. The middle sheet position and orientation errors, however, exceed 1 mm and 0.5 deg, respectively. These relatively large errors are due to flexibility in the suspension system, friction at wire supports, and large kinematic gains at extreme positions and indicate the need for middle sheet error measurement and feedback control.
[DOI: 10.1115/1.4044412]

Keywords: actuators and transmissions, cable-driven mechanisms, control, mechanism design, mechanism synthesis

1 Introduction

The cost of solar power has dropped drastically in recent years, encouraging record numbers of installations and the proliferation of this renewable energy source [1–3]. Concentrating photovoltaics (CPV) are twice as efficient as traditional photovoltaics (15% versus 30%) [4], but they require sun tracking. CPV systems work by concentrating and focusing the incoming light onto small and highly efficient solar cells. High-concentration (~100–1000×) requires very accurate tracking due to the low angular acceptance characteristics of the optics [5]. CPV systems are often relatively large, use dual-axis tracking mechanisms on top of pedestals, and need to be strong enough to maintain performance during wind loading. Thus, the tracking mechanism can be a significant portion of the system cost [6]. The CPV mechanism and structure require a large working volume that inhibits rooftop installation. The design needs to be reliable for the 25-year product lifespan of a typical solar panel system [4], longer than the lifetime of many electromechanical components that are continuously exposed to the environment.

Micro-optic solar concentrators use smaller optics to concentrate light onto individual cells or a shared photovoltaic (PV) cell. Hallas et al. [7] designed a system where the micro optics array focuses light onto a prism array that reflects the light to one edge of the array where a single PV cell harvests the energy. This system can be mounted on a two-axis rotating pedestal and controlled to maintain normal incidence with the sun. Alternatively, the optic array is fixed, but the prism array translates up to 4 mm in each direction with high precision to maintain alignment with the PV cell. Three cams driven by stepper motors control the position of the prism array [5].

Price et al. [4] describe a fully automated planar microtracking CPV system that is roof mounted and operates at a fixed tilt with microscale triple-junction solar cells at more than 660× concentration ratio over a 140-deg field of view. In this design, a transparent middle sheet with embedded microscale solar cells is sandwiched between a lenslet array on the top and a reflector array on the bottom and surrounded with refractive index matching fluid to remove reflections. The middle sheet moves during the day to align the solar cells with the incoming solar radiation. Experimental tests with a single cell demonstrated 50% more energy per unit area per day than a commercial silicon solar cell. However, this experiment used expensive high precision linear stages and no attempt was made to seal in the required refractive index matching fluid. Lloyd et al. [8] used a similar design but with magnets in the middle sheet to avoid sealing challenges, but had additional problems with stick-slip motion and limited positioning accuracy of 500 μm. An ideal tracking system for integration and installation would have the actuators sealed with the middle sheet and refractive index matching fluid, be lightweight, and maintain the slim (~1 cm) optical design.

Shape memory alloy (SMA) actuators are an attractive alternative to electric motors for solar tracking and have been considered in the past for rotational tracking systems [9–11]. With the additional constraints of a compact tracking mechanism, a sealed design, and panel integration, SMA is particularly attractive for CPV microtracking applications. Relative to electric motors, SMA actuators can be less expensive, more reliable, easily integrated, and consume lower power.[1] In addition, SMA actuators are easily maintained, provide clean and silent actuation, and controllable with simple (e.g., PID) feedback algorithms [12].

Contributed by the Mechanisms and Robotics Committee of ASME for publication in the Journal of Mechanisms and Robotics. Manuscript received December 28, 2017; final manuscript received July 25, 2019; published online August 1, 2019. Assoc. Editor: James J. Joo.

[1] http://www.dynalloy.com/pdfs/TCF1140.pdf

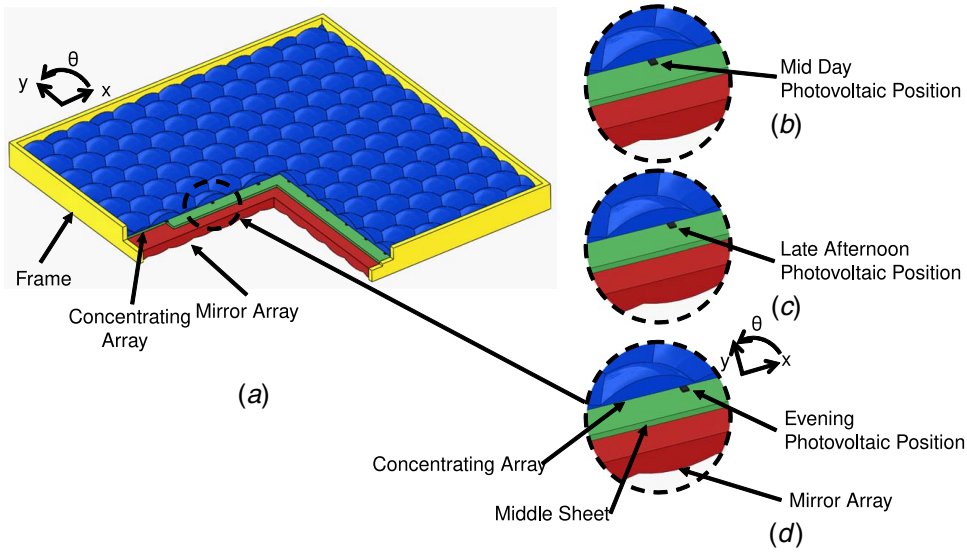

Fig. 1 Full-scale high-concentration microtracking photovoltaic system: (*a*) partial section view, (*b*) mid day, (c) late afternoon, and (*d*) late evening

This paper is the first to use SMA actuators for CPV microtracking applications. An SMA microtracking system is designed for a multicell CPV system based on the work of Ref. [4]. The kinematics using three SMA actuators and a passive spring are derived and a wide search for design alternatives is undertaken. Design constraints include the maximum and minimum force in the actuator wires and minimum actuated vertical and horizontal displacements and rotations.

2 Mechanical Design

2.1 Concentrating Photovoltaics Microtracking System Design. Figure 1(*a*) shows a conceptual drawing of the microtracking CPV design in Ref. [4] as envisioned for a panel with multiple solar cells. The structure has three layers: a top concentrating lenslet array, a transparent middle PV array, and a bottom mirror array. The system is surrounded by a small footprint frame to maximize the W/m^2, a key metric for solar panels. In this design, the frame, lenslet array, and mirror array are stationary. The lenslets and corresponding photovoltaic cells are hexagonally tilted with a distance of 14 mm on the long axis, and the complete optic is 9-mm thick. The photovoltaic cells are arranged in a grid pattern on the middle sheet. All three layers are made from transparent materials such as acrylic or glass. The lenslet and mirror arrays are molded to produce the desired optics and coated with anti-reflective and reflective layers, respectively. The middle sheet is sandwiched between the top and the bottom array and surrounded with index matching fluid to minimize refraction. Figure 1(*b*) shows that the PV cells are directly below the lenslets at noon with a perfectly tilted panel. The lenslets focus the sunlight onto the cells of size 650 μm × 650 μm. Due to the lenslet design, the solar cells need only to move laterally to stay within the focal point and the middle sheet tracks this motion keeping all PV cells in focus. The required displacement is roughly equal to the size of the lenslets and is independent of the size of the panel. For the purposes of this paper, we assume a ±7-mm motion requirement in the horizontal and vertical directions. With a full-size panel, up to 2 m in length, a small rotation of the middle sheet relative to the lenslet arrays causes the cells at the periphery to move outside of the focal point. Thus, accurate rotation control is also required. A typical solar panel for rooftop applications (1.7 m × 1 m) is much larger than the small prototype shown in Fig. 1, but the positioning requirements are the same except for slightly relaxed rotational tolerance in the prototype.

Figure 2 shows the design of the prototype CPV microtracking array studied in this paper. The concentrating lenslet array, middle sheet, and mirror array are stacked on the top of each other. The frame and frame cap secure the mirror and lenslet arrays, respectively; seal the index matching fluid using O-rings; and house the SMA actuators. Each of the three SMA wires is anchored to the frame at one end and attached to a secondary cable. The secondary cable is wrapped around an encoder shaft that measures the stroke of the SMA actuator. From the encoder, the secondary cable feeds through gaps in the mirror array and anchors to the middle sheet. Each SMA wire is electrically grounded near the encoder and connected to a controlled amplifier at the frame anchor. An additional cable (not shown in Fig. 2) attaches the middle sheet to a spring to ensure that all of the cables and SMA wires remain under tension during the operation. The frame has significant dead space to allow exploration of the design space without significant redesign. In an actual PV panel, the actuators and seals could be more tightly packaged to increase energy density.

2.2 Shape Memory Alloy Mechanism Design. Figure 3 shows that the middle sheet moves in x translation, y translation, and θ rotation, so three actuators are used to control these three degrees of freedom. The mechanism consists of three SMA links with variable lengths. Figure 3(*a*) shows the eight links and nine joints of the planar mechanism. Grübler Kutzbach analysis [13] calculates that this mechanism has three degrees of freedom, so the

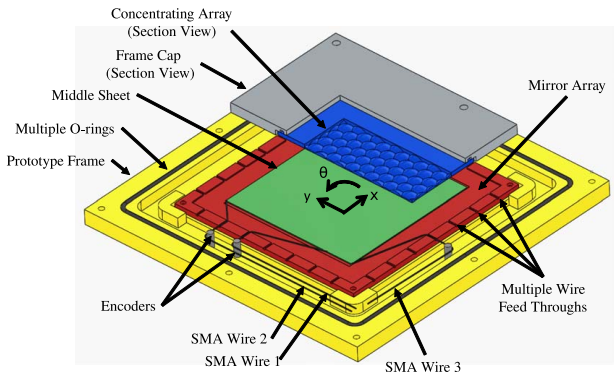

Fig. 2 CPV microtracking prototype design

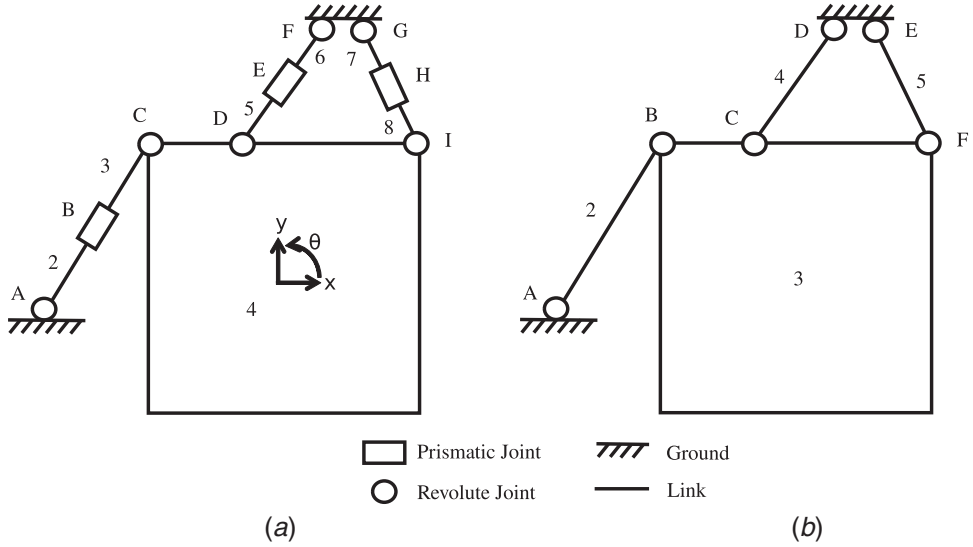

Fig. 3 Mobility analysis of the SMA planar mechanism concept: (*a*) variable link lengths and (*b*) fixed link lengths

middle sheet (link 4 in Fig. 3(*a*)) can translate in both planar directions and rotate. The mechanism in Fig. 3(*b*) corresponds to the system with five, fixed-length SMA links and six joints. Grübler Kutzbach analysis calculates that this mechanism has 0 degrees of freedom and is a structure. Thus, if the SMA lengths are regulated at a fixed value, the middle sheet will hold its position.

For the proposed optics, the middle sheet moves 14 mm in the x direction over 12 h as the sun rises and sets. The sun changes position in the sky during the year, and this requires y translation of the middle sheet. To allow complete coverage of the sky and flexibility of mounting orientation, the 14 mm x direction specification carries over to the y direction as well. SMA actuators are well suited to this slow but precise movement.

Figure 4 shows three SMA actuators and a spring pulling on the middle sheet to change its position/orientation and maintain tension in the cables, respectively. Three encoders measure the length of the SMA actuators. The device kinematics map the encoder measurements to middle sheet position and orientation, assuming straight and inextensible cables. The SMA actuators are resistively heated by the current flowing from fixed anchors connected to the amplifier input voltage through crimps to ground wires near the encoders. The crimps also attach the SMA wires to the secondary control wires that wrap around encoder shafts and run through a wire feedthrough in the frame to the middle sheet. Link 1 is the frame or ground, links 2, 4, and 5 are actuators, link 3 is the middle sheet, and link 6 is a tension spring. The simplicity of a single spring design is preferred, but more tension springs can be added if one is insufficient to maintain tension in all SMA wires at all positions of the middle sheet.

Figure 5 shows the middle sheet range of motion needed for the proposed optics. The points A through H are the extremes of the middle sheet position that give maximum flexibility in mounting orientation. The design of the proposed microtracking system involves ensuring the desired tracking of points A through H with 50-μm accuracy while maintaining cable tensions F_2, F_4, F_5, and

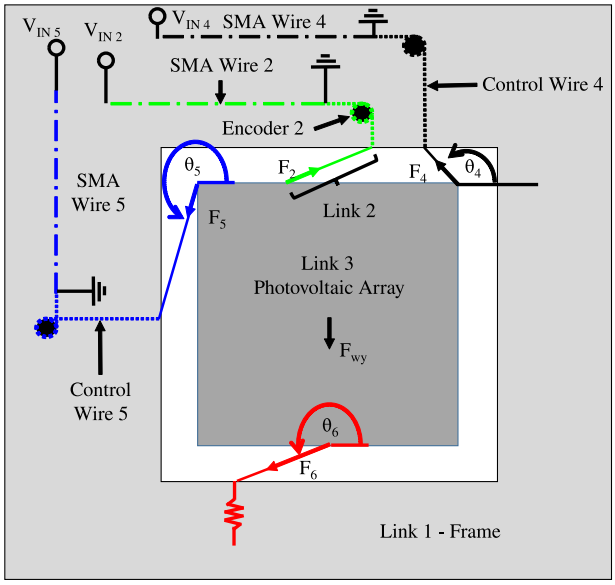

Fig. 4 CPV microtracking array position/orientation control hardware and free body diagram of the middle sheet

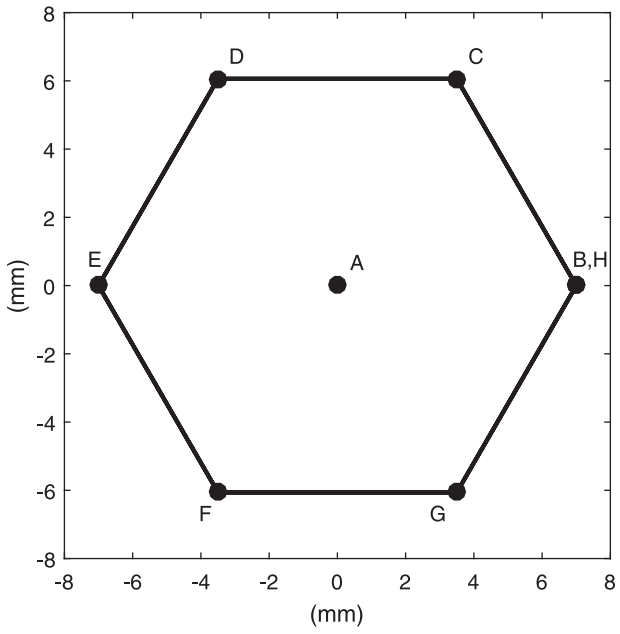

Fig. 5 Operating position envelope for the middle sheet

F_6 in a desired range. To maximize W/m^2, the gap between the middle sheet and the frame should be as small as possible. In this study, the middle sheet is scaled down from a typical 1.7 m × 1 m array to 140 mm × 140 mm for reduced complexity in a proof-of-concept device. Adding 14 mm of travel means the frame must be at least 154 mm × 154 mm. At the extremes of movement with this minimum clearance design, however, the transmission angles become large and the tension forces spike. Thus, the design includes a complex tradeoff between W/m^2 and SMA actuator size.

3 Detailed Design

3.1 Kinematic Solution. To find motion control solutions that meet the displacement and force requirements, the kinematics are solved numerically for millions of combinations of actuator link and spring link placements. The links are assumed to be distributed around the middle sheet as follows: one actuator on the left, two actuators on the top, and a tension spring on either the bottom or the right. All sides of the middle sheet and the frame are discretized into seven possible attachment points. Iterating through all attachment points on the frame and middle sheet for all four links produces millions of possible designs. The solutions were tested at all positions as displayed in Fig. 5.

The kinematic analysis is based on Haug [14], where the variables are defined as follows:

$r_i = [r_{ix}, r_{iy}]^T$	Global position of body i's origin
r_i^P	Global position of point P on body i
$s_i^{'P}$	Position of point P on body i measured from body i's origin
s_i^P	Position of point P on body i relative to body i's origin but measured using the global coordinate frame
Φ_i	Orientation for reference frame attached to body i
A_i	Orthonormal rotation matrix for body i

The rotation matrices transform from local to global coordinates

$$s_i^P = A_i s_i^{'P}$$

$$r_i^P = r_i + A_i s_i^{'P}$$

The frame is fixed at $r_1 = [0, 0]^T$ and $r_3 = [r_{3x}, r_{3y}]^T$ where r_{3x} and r_{3y} are the given locations of the center of the middle sheet relative to the center of the frame shown in Fig. 5. The kinematic equations for link 2 are given by

$$r_1^A = r_1 + A_1 s_1^{'A} \tag{1}$$

$$r_3^A = r_3 + A_3 s_3^{'A} \tag{2}$$

$$d_2 = r_3^A - r_1^A \tag{3}$$

$$L_2 = \| d_2 \| \tag{4}$$

$$\Phi_2^1 = \tan^{-1}\left(\frac{d_{2y}}{d_{2x}}\right) \tag{5}$$

$$\theta_2 = \Phi_2 + \pi \tag{6}$$

Vectors are similarly calculated for the other three links using Eqs. (1)–(6).

The free body diagram of the middle sheet shown in Fig. 4 is used to calculate the cable tensions and includes the gravitational load

$$F_{wy} = (mg - F_B)\sin(\Phi_{incline}) \tag{7}$$

The solar panel system will be installed at an angle $\Phi_{incline}$ so, for example, it is facing south if installed in the northern hemisphere. The middle sheet will be submerged in a refractive index matching fluid that produces a bouancy force F_B. The middle sheet weight (mg) is larger than F_B, so the mismatch will load the cable suspension.

The slow movement of the middle sheet means that a static analysis without fluid drag and friction is appropriate. Link 6 is a spring that tensions links 2, 4, and 5 with the tension force

$$F_6 = (L_6 - L_{6i})k_6 + F_{6i} \tag{8}$$

where F_{6i} and k_6 are the pretension and stiffness of the spring. Force and moment balances yield:

$$\sum F_x = F_2\cos(\theta_2) + F_4\cos W/m^2(\theta_4) + F_5\cos(\theta_5) + F_6\cos(\theta_6) = 0 \tag{9}$$

$$\sum F_y = F_2\sin(\theta_2) + F_4\sin(\theta_4) + F_5\sin(\theta_5) + F_6\sin(\theta_6) - F_{wy} = 0 \tag{10}$$

$$\sum M = \vec{r}_2 x\vec{F}_2 + \vec{r}_4 x\vec{F}_4 + \vec{r}_5 x\vec{F}_5 + \vec{r}_6 x\vec{F}_6 = 0 \tag{11}$$

$$\sum M = F_2[\sin(\theta_2),\ \cos(\theta_2)]s_3^{'A} + F_4[\sin(\theta_4),\ \cos(\theta_4)]s_3^{'C} + F_5[\sin(\theta_5),\ \cos(\theta_5)]s_3^{'B} + F_6[\sin(\theta_6),\ \cos(\theta_6)]s_3^{'D} = 0 \tag{12}$$

Figure 6 shows example forces in links 2, 4, 5, and 6. This design maintains all of the links in tension at all six points of the operating envelope. If the SMA forces are too high, however, the wires will not provide reliable and long-life operation. The SMA forces also cannot be too low or the SMA material will not transition properly to provide reversible actuation. The force window can be scaled by changing the wire diameter because the upper and lower limits are stress based. Figure 6 shows that using Dynalloy Flexinol® SMA wires with 0.51 mm diameter for link 2 and 0.38 mm diameter for links 4 and 5 will keep the stresses in all actuators in their desired ranges (8–20 N

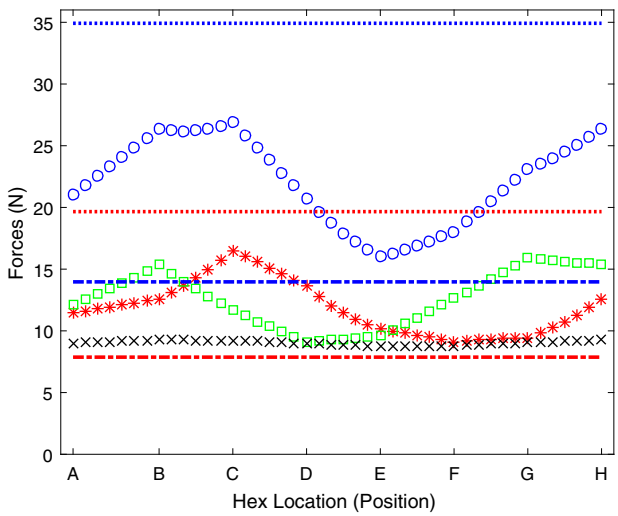

Fig. 6 Static forces for an example configuration at positions A–F shown in Fig. 5: links 2 (○), 4 (*), 5 (□), and 6 (x). Maximum and minimum forces are the dotted and dash-dotted lines, respectively, for 0.51-mm (blue) and 0.38-mm (red) diameter Dynalloy SMA wire. (Color version online.)

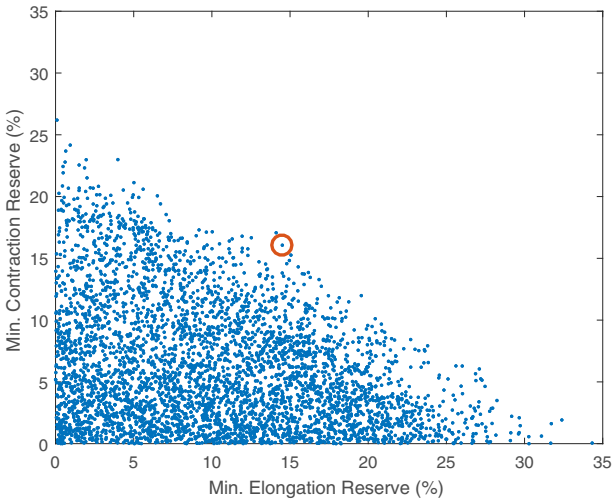

Fig. 7 Minimum and maximum strain reserves for design candidates (blue dots) and design point (red circle) (Color version online.)

and 14–35 N for the 0.38- and 0.51-mm diameter wires, respectively)[2] ensuring reversible actuation for millions of cycles. Each SMA actuator goes through one actuation cycle each day for 25 years, so the cycle count would be well below the millions of cycles advertised by Dynalloy for their Flexinol® product.

In general, the forces in the three SMA actuators increased as the mechanism approached a less stable configuration, where the determinate of the kinematic Jacobian was closest to zero, and these designs did not meet the specifications. Positions B, C, G, and H were less stable than the rest of the positions, but the mechanism performed stably throughout the workspace for designs meeting the specifications.

Wire feedthroughs were placed every 25 mm around the perimeter of the mirror array as shown in Fig. 2. These openings provided a fixed number of mechanism geometry combinations. A brute force approach was used to analyze all possible combinations using three SMA actuators and one return spring. More than one spring was considered but using only one spring resulted in a simpler design which met the design criteria. Figure 7 shows the 8504 designs that meet Flexinol® wire specifications for maximum and minimum strains based on the reserves

$$R_{\text{elongation}} = \left(\frac{F_{2\min} - F_{e1}}{F_{e1}}\right)100\% \tag{13}$$

$$R_{\text{contraction}} = \left(\frac{F_{c1} - F_{2\max}}{F_{c1}}\right)100\% \tag{14}$$

where $F_{2\min}$ and $F_{2\max}$ are the minimum and the maximum tensions in the SMA actuator for all positions, respectively, and F_{e1} and F_{c1} are the Dynalloy recommended minimum and maximum tensions, respectively, for the given diameter wire. The red-circled dot in Fig. 7 is the chosen design point. This solution provides favorable reserves for both the elongation and the contraction of the SMA actuator.

Once the wire diameter has been chosen to meet the stress limits, wire length is scaled to provide the desired displacement. Flexinol® wires can reliably produce 3% strain for millions of cycles.[3] The maximum link change in length for the final design was 13.2 mm. This stroke was 3% strain for a 440 mm SMA actuator, but the wire length was increased to 500 mm to provide an additional actuation margin.

[2]See Note 1.
[3]See Note 1.

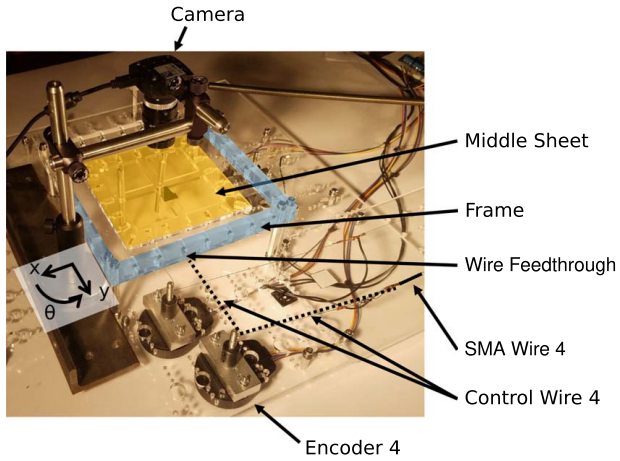

Fig. 8 Kinematic prototype tested in this paper

The final design is shown schematically in Fig. 4 and photographically in Fig. 8. The left SMA wire (link 5) attaches to the upper left corner of the middle sheet and passes through the middle slot in the left side of the frame. The first top control wire (link 2) attaches near the middle of the top of the middle sheet and passes through the frame near the top middle. The second top control wire (link 4) attaches to the top-right corner of the middle sheet and passes through the frame near its top-right corner. The spring attaches to the bottom near the middle of the middle sheet and passes through the left side of the bottom of the frame. This design provides both clockwise (CW) and counterclockwise (CCW) moments and $\pm x$ and $\pm y$ translations with all wires under tension at all locations. The actuator for link 2 is 0.51 mm diameter SMA wire, while links 4 and 5 both use actuators with 0.38 mm diameter wire. Figure 8 shows the middle sheet, frame, SMA actuators, encoders, and spring used for the fabricated prototype.

4 Control

4.1 Implementation. Middle sheet position control is implemented on an Ardunio Uno microcontroller. Three 40,000 count/revolution encoders measure the SMA wire lengths and provide the information to the microcontroller using pulse count modules by GHI Electronics and a serial peripheral interface. Three pulse width modulation (PWM) outputs from the microcontroller are amplified to heat the SMA actuators resistively. Previous work on SMA has shown that PWM-modulated control can reduce power consumption by up to 30% compared with the continuous control [15].

4.2 Proportional Integral Derivative Control Design. PID controllers provide middle sheet position control by regulating the length of all the three actuators. The controllers are decoupled and use only feedback from their respective encoders. The control objective is to move the middle sheet in the x and/or y directions without rotation. To convert the desired x, y, and θ middle sheet position and orientation to link length commands, the kinematics are quasi-linearized using:

$$G_i = \frac{\Delta L_i}{\Delta x} \tag{15}$$

where the current position and orientation vector $x = [x, y, \theta]^T$, Δx is the desired change in position and orientation, and ΔL_i the resulting change in link L_i length. The gradient vector $G_i = [G_{ix}, G_{iy}, G_{i\Phi}]^T$ is calculated and stored on the microcontroller for all points on a grid pattern of 1 mm × 1-mm spacing within the hexagonal positioning envelope as shown in Fig. 5. Quasi-linearization is appropriate for small changes in a configuration that would typically be required during solar tracking.

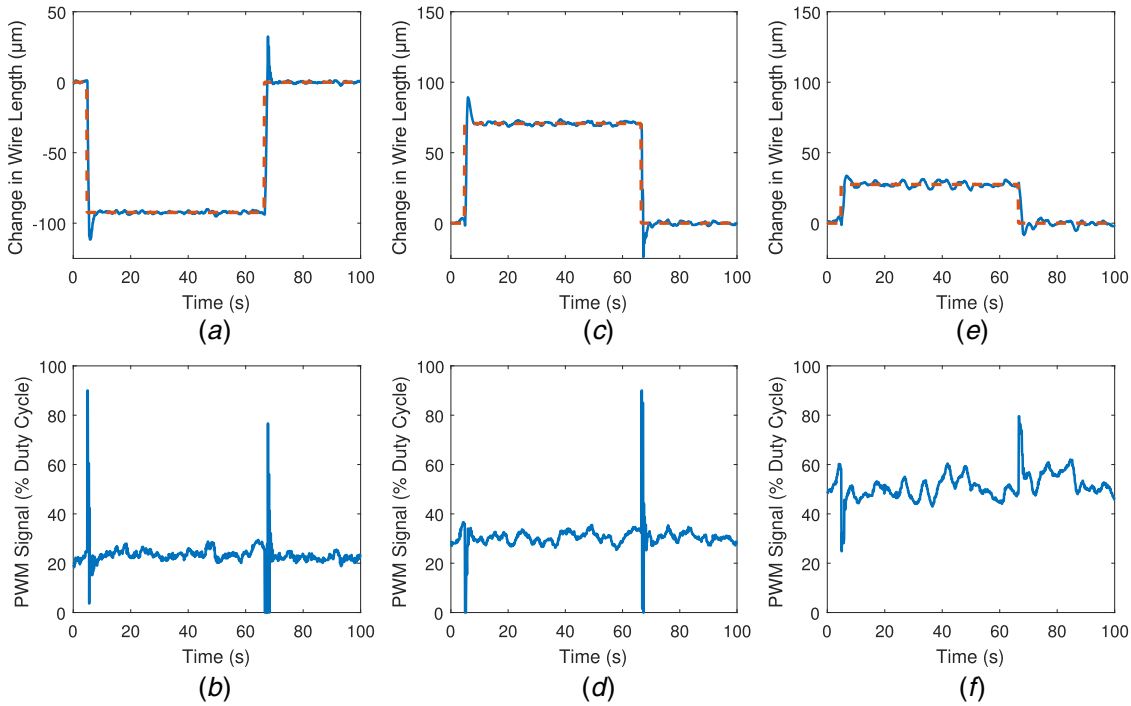

Fig. 9 PID control response for a 100 μm × translation: (*a*) desired (red-dashed line) and actual trajectory (blue solid line) and (*b*) PWM signal for link 2; (c) desired (red-dashed line) and actual trajectory (blue solid line) and (*d*) PWM signal for link 4; and (e) desired (red-dashed line) and actual trajectory (blue solid line) and (*f*) PWM signal for link 5 (Color version online.)

4.3 Dynamic Response. Figure 9 shows a typical movement of the middle sheet, a 100 μm translation in the x direction starting at the center location. The responses of links 2, 4, and 5 are shown with the desired length calculated from Eq. (15) (dashed) and the actual response (solid). Link 2 contracts while links 4 and 5 extend to enable the middle sheet to move horizontally without vertical translation or rotation.

The time response results are summarized in Table 1 for each SMA actuator and the overall middle sheet position control performance. The response differs for contraction versus elongation of the SMA wire because resistive heating is faster than passive cooling. The calculated time constant is twice as slow for cooling as heating except for SMA actuator 5. Responding in one second, however, is sufficiently fast for the slow solar tracking application. While the overshoot is somewhat large due to relatively large gains and aggressive integral action, the steady-state error is the most important to keep the focal point focused on the PV cell. The cell is roughly 650 μm^2 and so 6.93 μm of steady-state error is quite small. SMA actuators 4 and 5 have the same PID gains; however, their response is quite different. This is due to the dynamic differences between the two actuator interfaces.

4.4 Calibration and Kinematic Performance. The time response results presented in the Sec. 4.3 pertain to the measured SMA link lengths, not the position and the orientation of the middle sheet. The flexibility of the cable suspension of the middle sheet and other factors contribute to positioning errors even if the links are exactly of the right lengths. To assess the significance of these errors, a high-resolution camera (THORLABS DCC1645C) with a 12× lens (NAVITAR 12-1248) mounted 60 mm above the middle sheet captures digital images that are processed to measure translation and rotation. The resolution is limited to 0.03 mm for translations and 0.13 deg for rotation.

Table 2 shows the measured errors for position control at the center and around the periphery of the hexagonal envelope in Fig. 5. The test starts at the center with the displacement and rotation defined to be zero. After touching all points of the hexagon, the middle sheet returns to the origin, showing relatively small translational errors of 150 μm and rotational errors of 0.13 deg. At the periphery, however, the position errors exceed 1 mm and orientation errors are near 1 deg. The PV cells are 650 μm × 650 μm so errors this large would move the focal point outside the cell, minimizing power generation. For a full-scale solar panel, rotation errors are the most significant for the cells that are on the edge of the panel. Maintaining less than 650 μm in displacement error for a 1.7-m panel, for example, requires rotation errors less than 0.02 deg. The system design could be modified to reduce these errors by minimizing control wire stretch and bending angles, both of which contribute to flexibility between the control wire attachment point and

Table 1 PID controller performance for SMA actuator wire #2

Step	Actuator response	Time constant (sec)	Overshoot (%)	RMS error (counts)	RMS error—actuator length (μm)	RMS error—photovoltaic × movement (μm)
100 μm + x	Actuator 2	0.34	21%	1.9	0.80	0.86
100 μm − x	Actuator 2	0.7	35%	1.5	0.62	0.67
100 μm + x	Actuator 4	0.61	35%	2.5	1.07	1.51
100 μm − x	Actuator 4	0.39	66%	2.1	0.89	1.26
100 μm + x	Actuator 5	1	30%	4.5	1.90	6.93
100 μm − x	Actuator 5	1.1	54%	3.7	1.56	5.70

Table 2 Middle sheet position and orientation errors under PID control

Position	Desired location (mm)		Measured location (mm)		X Error (mm)	Y Error (mm)	Rotational error (deg)
A	0	0	0	0	0	0	0
B	7	0	6.45	−0.17	−0.55	−0.17	0.13
C	3	6	1.89	5.55	−1.11	−0.45	0.78
D	−3	6	−3.19	5.89	−0.19	−0.11	0.13
E	−7	0	−6.07	0.23	0.93	0.23	−0.39
F	−3	−6	−2.79	−5.78	0.21	0.22	0.00
G	3	−6	2.27	−5.92	−0.73	0.08	0.13
B	7	0	6.24	−0.23	−0.76	−0.23	0.39
A	0	0	−0.15	0.00	−0.15	0.00	0.13

the measured SMA wire connection. A direct measurement of the middle sheet position, such as with capacitive displacement sensors embedded in the middle sheet, can also be used to calculate the control wire lengths and adjust the SMA wires accordingly, resulting in less positioning error.

The tracking system is designed to follow the sun autonomously and feedforward information based on the date, location, and time of day could be used to roughly position the middle sheet. Offset photovoltaic cell feedback can then be used to center the energy harvesting PV cells in the concentrated light continuously throughout the day. Positioning the middle sheet without these offset photovoltaic cells, or similar additional feedback system, is not feasible for the current design.

4.5 Power Consumption. Assuming a solar irradiance of 1000 W/m^2, a CPV panel with 30% power conversion efficiency and 1-m^2 area would produce 300 W. The SMA actuators consume a combined total of 8.5 W on the scaled prototype during typical operation of holding the position, less than 3% parasitic power loss. The motion requirements will not scale with the panel size, so these numbers hold for the full-scale device. SMA wires require continuous resistive heating to compensate for the heat loss, maintain the temperature, and regulate the length. A simple felt insulation sleeve was installed around the SMA actuator wire, and the power decreased by more than 20%, so insulation, while slowing the cooling response, can reduce power consumption. In addition, the kinematic geometry selected was optimized for reserves. The geometry can be optimized for power consumption by lowering the forces and selecting smaller diameter SMA actuator wires. A NEMA 8-size stepper motor with 200 steps per revolution attached to a 64:1 gear ratio gearbox has sufficiently small steps (equivalent to 3.125 steps per encoder count) and high torque to drive the encoder shafts and would consume 3.6 W. Thus, three stepper motors would consume slightly more power than the uninsulated SMA actuator wire design.

5 Conclusion

Using SMA actuator wires for high-concentration microtracking PV systems is viable for low-profile and high W/m^2 solar panels that can be installed flat on rooftops. With three 0.5 m long SMA actuator wires and a passive spring, the middle sheet can completely traverse the solar cell dimensions and maintain desired tension levels. The SMA actuator wires under quasi-linearized PID control demonstrate a steady-state stroke error of 1.9 μm, over 300 times smaller than the solar cell size. Middle sheet position and orientation control are insufficient, however, due to flexibility in the cable suspension system. The speed of response is very fast relative to the slow movement of the sun. Future work includes optimizing the kinematic geometry and SMA actuator wire selection for power consumption and/or higher stiffness suspension of the middle sheet and using a middle sheet and/or solar error feedback to improve the position and orientation control. In addition, the SMA actuators and springs will need to be scaled up for a typical full-size 1.7 m^2 CPV array that can function at a range of installed angles associated with different roof slopes, orientations, and physical locations.

Funding Data

- Advanced Research Projects Agency-Energy (Grant No. DE-AR0000626; Funder ID: 10.13039/100006133).

References

[1] Green, M. A., 2016, "Commercial Progress and Challenges for Photovoltaics," Nat. Energy, **1**, pp. 15015.
[2] Lewis, N. S., 2016, "Research Opportunities to Advance Solar Energy Utilization," Science, **351**(6271), p. 353.
[3] Woodhouse, M., Jones-Albertus, R., Feldman, D., Fu, R., Horowitz, K., Chung, D., Jordan, D., and Kurtz, S., 2016, "On the Path to SunShot: The Role of Advancements in Solar Photovoltaic Efficiency, Reliability, and Costs," National Renewable Energy Laboratory, Golden, CO, NREL/TP-6A20-65872. https://www.nrel.gov/docs/fy16osti/65872.pdf
[4] Price, J. S., Grede, A. J., Wang, B., Lipski, M. V., Fisher, B., Lee, K., He, J., Brulo, G. S., Ma, X., Burroughs, S., Rahn, C. D., Nuzzo, R. G., Rogers, J. A., and Giebink, N. C., 2017, "High-Concentration Planar Microtracking Photovoltaic System Exceeding 30% Efficiency," Nat. Energy, **2**(8), p. 17113.
[5] Baker, K. A., Karp, J. H., Tremblay, E. J., Hallas, J. M., and Ford, J. E., 2012, "Reactive Self-Tracking Solar Concentrators: Concept, Design, and Initial Materials Characterization," Appl. Opt., **51**(8), p. 1086.
[6] Hallas, J. M., Baker, K. A., Karp, J. H., Tremblay, E. J., and Ford, J. E., 2012, "Two-Axis Solar Tracking Accomplished Through Small Lateral Translations," Appl. Opt., **51**(25), p. 6117.
[7] Hallas, J. M., Karp, J. H., Tremblay, E. J., and Ford, J. E., 2010, "Lateral Translation Micro-Tracking of Planar Micro-Optic Solar Concentrator," Proc. SPIE, **7769**, p. 776904.
[8] Lloyd, J., Pavilonis, M., Gladden, C., Casper, C., Schneider, K., McMahon, W., and Kozodoy, P., 2018, "Performance of a Prototype Stationary Catadioptric Concentrating Photovoltaic Module," Opt. Express, **26**(10), p. A413.
[9] Poulek, V., 1994, "Testing the New Solar Tracker With Shape Memory Alloy Actors," Proceedings of 1994 IEEE 1st World Conference on Photovoltaic Energy Conversion—WCPEC, Waikoloa, HI, Dec. 5–9, 1994, p. 1131.
[10] Degeratu, S., Alboteanu, L., Rizescu, S., Coman, D., Bizdoaca, N. G., and Caramida, C., 2014, "Active Solar Panel Tracking System Actuated by Shape Memory Alloy Springs," International Conference on Applied and Theoretical Electricity (ICATE), Craiova, Oct. 23–25.
[11] Ganesh, N. J., Maniprakash, S., Chandrasekaran, L., Srinivasan, S. M., and Srinivasa, A. R., 2011, "Design and Development of a Sun Tracking Mechanism Using the Direct SMA Actuation," ASME J. Mech. Des., **133**(7), p. 075001.
[12] Elahinia, M. H., and Ashrafiuon, H., 2002, "Nonlinear Control of a Shape Memory Alloy Actuated Manipulator," ASME J. Vib. Acoust., **124**(4), p. 566.
[13] Wohlhart, K., 1996, "Kinematotropic Linkages," *Recent Advances in Robot Kinematics*, Springer Netherlands, Dordrecht, pp. 359–368.
[14] Haug, E. J., 1989, *Computer Aided Kinematics and Dynamics of Mechanical Systems*, Allyn and Bacon, Boston, MA, pp. 32–34.
[15] Ma, N., and Song, G., 2003, "Control of Shape Memory Alloy Actuator Using Pulse Width Modulation," Smart Mater. Struct., **12**(5), p. 712.